The Journal of Experimental Biology 211, 215-223
Published by The Company of Biologists 2008
doi:10.1242/jeb.007823

Research article

The implications of low-speed fixed-wing aerofoil measurements on the analysis and performance of flapping bird wings

G. R. Spedding[1,*], A. H. Hedenström[2], J. McArthur[1] and M. Rosén[2]

[1]Aerospace and Mechanical Engineering, University of Southern California, Los Angeles, CA 90089-1191, USA and [2]Department of Theoretical Ecology, Lund University, SE 223-62, Lund, Sweden

*Author for correspondence (e-mail: geoff@usc.edu)

Accepted 23 May 2007

Summary

Bird flight occurs over a range of Reynolds numbers (*Re*; $10^4 \leqslant Re \leqslant 10^5$, where *Re* is a measure of the relative importance of inertia and viscosity) that includes regimes where standard aerofoil performance is difficult to predict, compute or measure, with large performance jumps in response to small changes in geometry or environmental conditions. A comparison of measurements of fixed wing performance as a function of *Re*, combined with quantitative flow visualisation techniques, shows that, surprisingly, wakes of flapping bird wings at moderate flight speeds admit to certain simplifications where their basic properties can be understood through quasi-steady analysis. Indeed, a commonly cited measure of the relative flapping frequency, or wake unsteadiness, the Strouhal number, is seen to be approximately constant in accordance with a simple requirement for maintaining a moderate local angle of attack on the wing. Together, the measurements imply a fine control of boundary layer separation on the wings, with implications for control strategies and wing shape selection by natural and artificial fliers.

Key words: animal flight, aerofoil, lift-drag polar, wake analysis, Reynolds number.

Introduction

Bird flight performance envelope

The equations of motion for a homogeneous, incompressible fluid with constant density, ρ, can be expressed so that, in the absence of any special boundary conditions, their solution for a given geometry depends only on the magnitude of one dimensionless number, the Reynolds number *Re*, which may be written as:

$$Re = \rho u l / \mu \,, \quad (1)$$

where u is a flow speed, l is a characteristic length scale and μ is the fluid viscosity. The numerator depends on the mass, size and speed at which fluid is moving, and one may think of *Re* as a measure of the relative importance of inertial and viscous forces in a flow. Inertial forces tend to destabilise a flow, while viscosity tends to smooth it out, and so high Reynolds numbers are frequently associated with complex, and possibly turbulent, flows. *Re* is a large number in many human-engineering applications. For example, for a large passenger plane (such as the Boeing 747-400) with cruising flight speed U=250 m s^{-1} and mean chord length c=8 m, a Reynolds number that uses c as the length scale is approximately 10^8. This is a large number, and one might expect the air motions to be characterised by enormously complex, turbulent flows. Indeed they are in the wake of the wings and body, but paradoxically enough, in the design and analysis of wing performance, the huge values of *Re* make it possible to completely ignore viscous terms, and a large and successful body of engineering literature makes accurate calculations of the aerodynamic performance based on inviscid (no viscosity) theories.

By contrast, birds are significantly smaller, and move more slowly, so that the typical *Re* based on mean chord shown in Fig. 1 is much lower, by three orders of magnitude or more, ranging from 10^4 to 10^6 as the body mass, m, varies from less than 10 g to over 10 kg. This can give rise to certain difficulties in applying formulae straight from aeronautics texts to bird flight, even while ignoring the fact that bird wings flap and deform in ways that are quite outside the usual engineering experience.

Wing performance at low Reynolds number

Because aeronautics is usually practised at much higher *Re* than appears in Fig. 1, relevant wing performance data are more scarce, and the few reliable sources (such as Althaus, 1980; Schmitz, 1945; Hoerner, 1965; Laitone, 1997) are limited in scope. Fig. 2 is taken from a comprehensive collection of aerofoil data (Lyon et al., 1997), and shows an example of the measured performance of a two-dimensional airfoil section at *Re* from 6×10^4 to 3×10^5. The aerofoil section is the Eppler 387, designed for sailplanes in what is termed low-speed flight in engineering literature. When *Re* falls significantly below the design space for this aerofoil (i.e. when $Re<10^5$), the lift:drag polars are characterised by a 'tongue', where at moderate angles of attack, α, the drag increases abruptly with little increase in lift. As α increases further, the drag decreases again, just as abruptly. The magnitude of the effect increases as *Re* decreases, and reasonable agreement (say, to within a factor of two for the drag) between different wind tunnel facilities is hard to find. The reason for the abrupt increase, and subsequent decrease of the drag with α, is due to the dynamics of a separation region on the upper (suction) surface of the aerofoil. The separation region may be associated with complete detachment of smooth streamlines from the aerofoil, but for a small range of α, the flow may reattach again, when the affected region is called a separation bubble. This

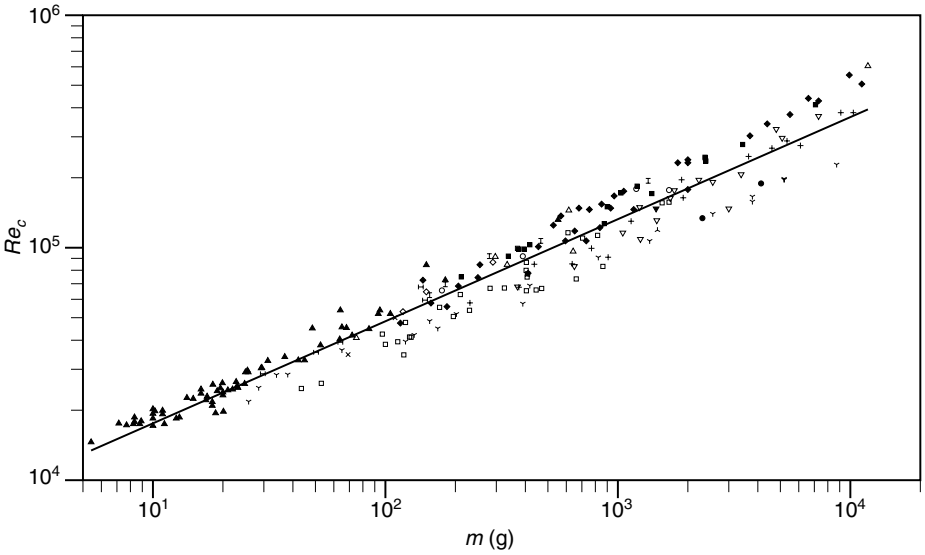

Fig. 1. Reynolds number *Re* based on wing chord *c* as a function of body mass *m* for birds. Data collected and selected by C. J. Pennycuick (personal communication). The different symbols represent different orders, and passerines are noted by filled upright triangles.

process of separation and possible reattachment is very sensitive to details in the aerofoil geometry, ambient turbulence and possibly $\alpha(t)$. Some kind of large amplitude variation in $C_d(\alpha)$ (C_d is a section lift coefficient of normalised lift per unit span, used for two-dimensional aerofoils; the coefficient of lift for a finite span wing is denoted C_D) is not uncommon at $Re \leqslant 10^5$ for smooth aerofoils with significant thickness. Because the physical process depends on small details of the viscous boundary layer, these flows are also very difficult to compute, and standard inverse methods of aerofoil design that either completely ignore viscous effects, or model them in an *ad hoc* fashion, fail completely.

Objectives

It is interesting that, as shown in Figs 1 and 2, a substantial fraction of birds operate within a Reynolds number regime where significant aerodynamic performance variation due to the presence or absence of boundary layer separation and/or reattachment can be predicted for fixed wings. The purpose of this paper is to evaluate recent results from wind tunnel studies of flapping bird flight in the light of companion studies on fixed wing performance. We investigate the degree to which the bird flight results can be understood in the light of the new fixed wing data, with a view to understanding how birds manage their aerodynamics in a potentially unstable or unpredictable flow regime.

Materials and methods

Wind tunnel facilities

The wind tunnel at Lund has been described in detail (Pennycuick et al., 1997), the set-up for recent DPIV-based measurements has been detailed previously (Spedding et al., 2003a; Spedding et al., 2003b). The facilities at the Dryden tunnel at University of Southern California (USC) have also been described (Spedding et al., 2006). Both tunnels have closed-loop designs, and large contraction ratios (12.25:1 at Lund; 7:1 at USC) that follow a series of smoothing screens (5 in Lund, 11 at USC). Consequently, the turbulence levels in both tunnels are quite low. For all experiments reported here, the tunnels operated at speeds from 5–10 m s^{-1}, when mean turbulence levels, u'/U, where u' is an averaged root mean squared fluctuating velocity and U is the mean speed, were approximately 0.035% (Lund) and 0.025% (USC). The comparatively low turbulence levels are essential for obtaining reliable force balance and wake measurements in the *Re* regime 10^4–10^5.

The birds in the Lund facility are trained to fly centred on a luminescent marker in reduced light conditions. Their wakes are sampled far downstream, 17–22 chord lengths aft of the bird, because of safety concerns with the high intensity laser light. In the USC tunnel, a wing is mounted vertically on a single sting connected to a custom force balance capable of resolving lift and drag forces of 0.1 mN (about 0.01 g force). The suspension system is damped so only time-averaged forces can be measured. Flow measurements are made on the suction surface, and at x=1c and 10c, where the x (streamwise) coordinate begins at the leading edge of the wing, with mean chord c. Measurements were made at various spanwise (y) locations in both sets of experiments. In the Lund tunnel this is done by monitoring the naturally occurring drift of the bird with respect to the light slice with a synchronised CCD camera placed in the downstream diffuser section, while in the USC tunnel, the light slice is simply moved along the fixed wing. The

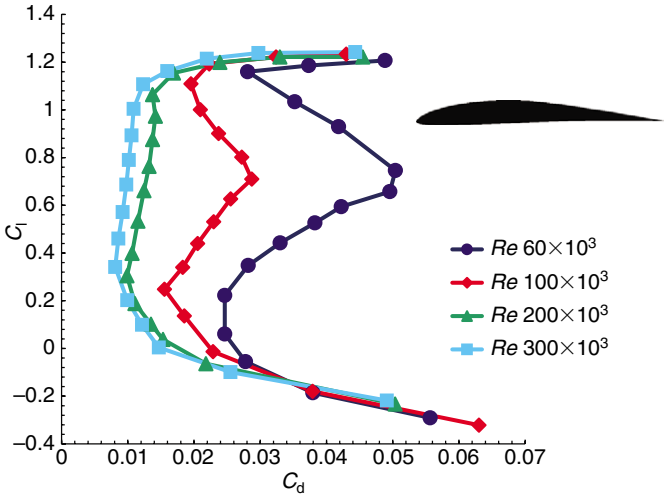

Fig. 2. Section lift:drag (C_l:C_d) polars for the Eppler 387 aerofoil (black silhouette), for angle of attack α from –4° to +11°. Replotted from data in Lyon et al. (Lyon et al., 1997).

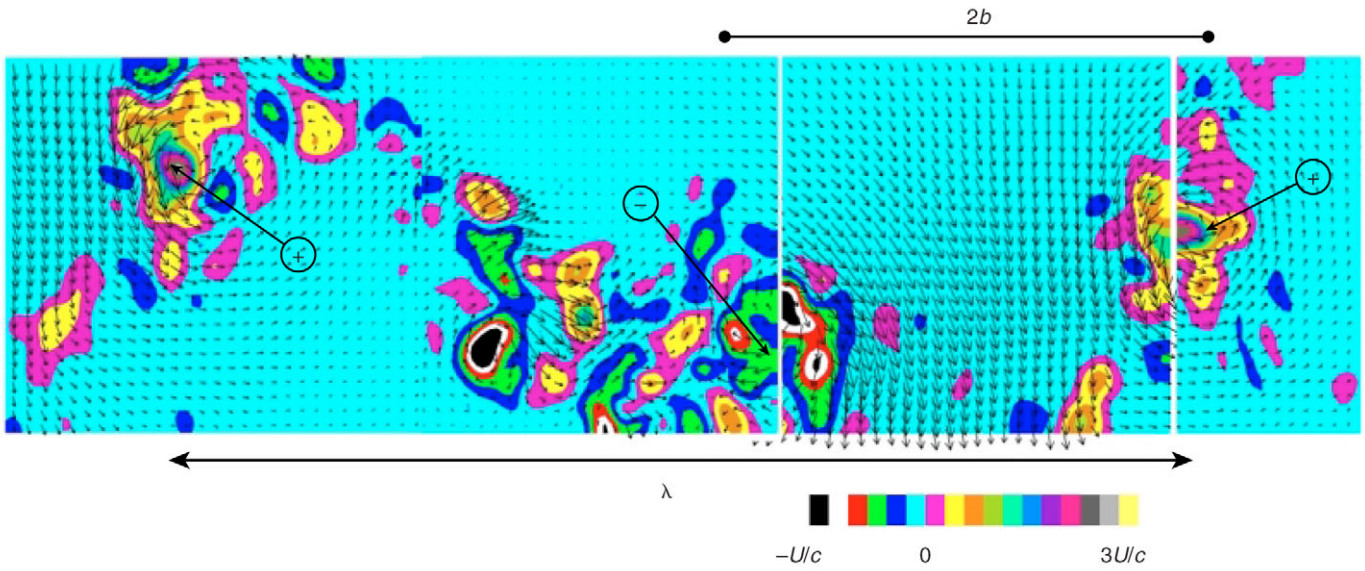

Fig. 3. Spanwise vorticity, $\omega_y(x,z)$ for a mid-wing slice taken at x=17c for the thrush nightingale in the Lund wind tunnel. The reference frame moves with the mean flow, as for flight from right to left through still air. A sequence of four frames from consecutive wing beats is collected to cover just over one wake wavelength (λ). + signs show patches positive vorticity shed at the beginning of the downstroke; there are two in this sequence. The equivalent patch of negative vorticity, noted by the – sign, is much more diffuse. From the same dataset (but a different sample) as Spedding et al. (Spedding et al., 2003b).

results here are given for rectangular planform wings with aspect ratio AR=2b/c=6 (where b is the wing semispan), and are for data taken at midspan.

Digital particle image velocimetry (DPIV) methods and data analysis

In both tunnels, a custom correlation imaging velocimetry (CIV) method (Fincham and Spedding, 1997; Fincham and Delerce, 2000) was used to estimate velocity fields in vertical light slices, aligned in the streamwise direction behind the wings. The recirculating tunnels were gradually filled with a fine smoke composed of 1 μm diameter particles. The particle image sizes and brightness were significantly improved after an hour or more of continuous operation, and this was systematically included in the experimental protocol. For a given lighting and particle set-up, the one remaining parameter is the CIV exposure time, δt, determined by the time difference between consecutive flashes of the dual-head Nd:Yag lasers. In the USC experiments, this varied between 100–300 μs; in the Lund wind tunnel it varied from 200–500 μs. For a given optical geometry, the correct choice depends on the flow complexity, both within and across the plane of the light slice, and significant differences in background noise can be realised with only a 20 μs change in δt.

The application of CIV techniques to these data have been described (Spedding et al., 2003a; Spedding et al., 2006) and will not be repeated in detail here. The important general operational consideration is that the correct tuning of the δt parameter can be matched by independent selection of correlation and search box sizes in the CIV algorithms so as to maximise the bandwidth of the velocity estimates about the likely range of disturbance values (with any mean flow subtracted) of the computed displacement field. Finally, the displacement field is reinterpolated onto a regular rectangular grid with patched smoothing spline functions, which can be differentiated analytically to yield the first order spatial derivatives. This operation also corrects for the finite displacement of velocity vectors during the exposure time δt. All the data described here come from estimates of the u and w velocity components in the streamwise (x) and vertical (z) directions, respectively. The rotational part of the velocity field is then given by the spanwise vorticity, denoted:

$$\omega_y = \frac{\partial w}{\partial x} - \frac{\partial u}{\partial z} \quad . \tag{2}$$

This quantity is displayed on discrete colour bars whose resolution reflects the uncertainty of the measurement. Very approximately, velocity estimates are likely to be correct within 1% and gradient quantities such as ω_y have a likely uncertainty of 5–10%.

Results

Wakes of birds and fixed wings

A number of recent studies have investigated the wakes of birds in the Lund wind tunnel (Spedding et al., 2003b; Rosén et al., 2004; Hedenström et al., 2006a; Hedenström et al., 2006b; Rosén et al., 2007). The birds range in mass from the thrush nightingale *Luscinia luscinia* (m=30.5 g) to the robin *Erithacus rubecula* (m=16.5 g). Their small size makes them good subjects for wind tunnel study as the corrections required for tunnel blockage and wake–wall interference are negligible. As measurements are made from 17–22c downstream, interpretation of the wake vorticity patterns is complicated by the fact that they have been evolving and deforming over this distance. Fig. 3 shows a vertical slice, aligned with the mean flow, in a plane at about the mid-semispan position. It is a composite from four consecutive frames, where slightly different phases of the wing beat (the wing-beat frequency, f=14 Hz, while the laser repetition rate is 10 Hz) are sampled at a fixed position in space. The data are shown in a reference frame moving with the mean flow, with vectors of the disturbance velocity shown at half resolution. The flight speed U, determined by the independently controlled tunnel speed, is 7 m s^{-1}, which can be regarded as close to a cruising speed. The spanwise vorticity, $\omega_y(x,z)$, is shown on a discrete colour bar, where light blue is zero and *extrema* are

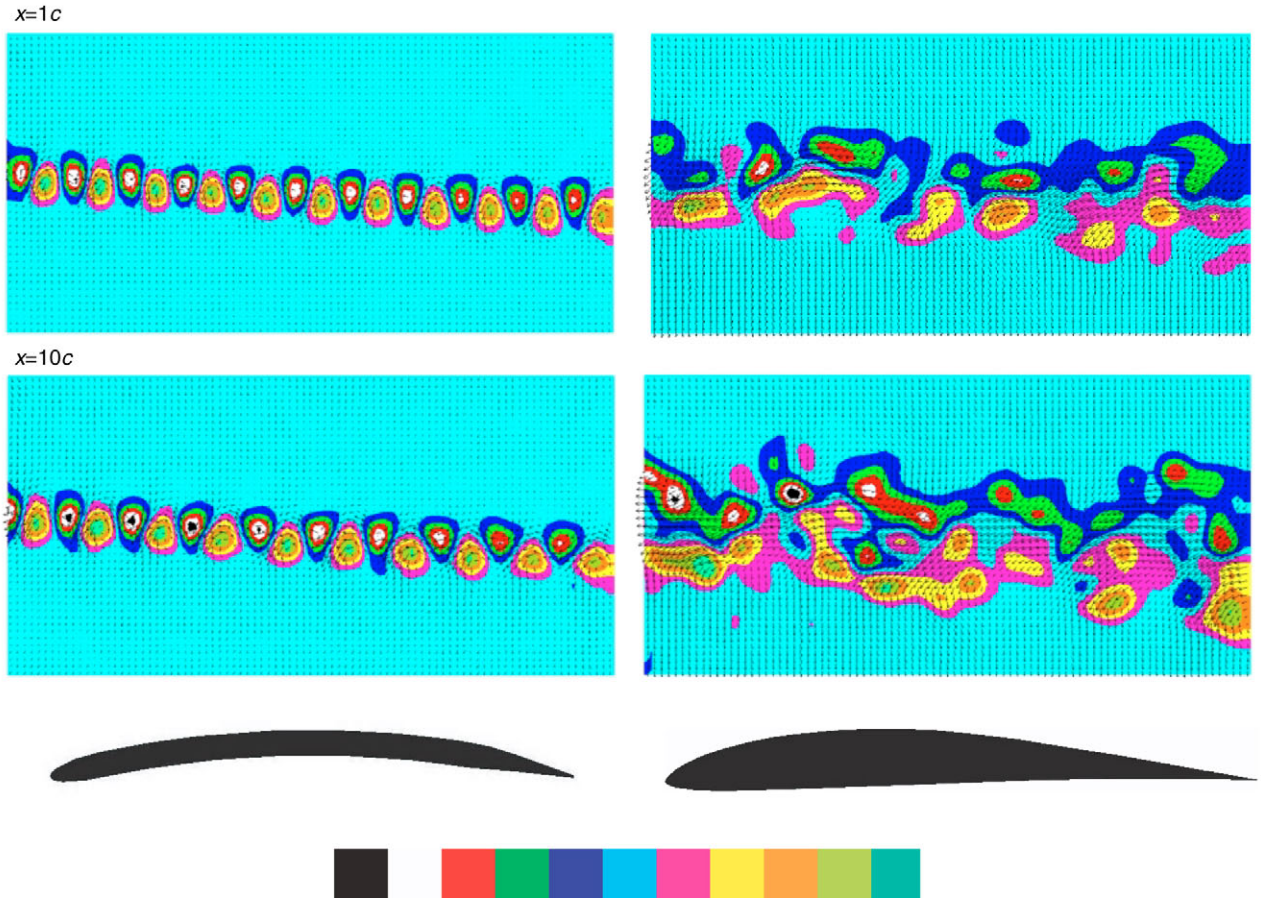

Fig. 4. Spanwise vorticity, $\omega_y(x,z)$ for two fixed wings, shown at midspan. The left column shows the wake for a thin cambered plate, with circular arc, and the right column is for the Eppler 387. The silhouettes are shown below. The top row is for a measurement station where the left margin is at $x=1c$ (immediately behind the trailing edge), and the symmetric colour bar is scaled to $\pm 8U/c$. The bottom row is taken at $x=10c$, and the colour bar is scaled to $\pm 2U/c$. The field of view is $3.2c \times 1.5c$ in x and z. The aerofoils are at fixed angle of attack, $\alpha=4°$, and the chord Reynolds number is 11.7×10^3.

mapped asymmetrically about this level. As has been noted before, the patches of spanwise vorticity that can be traced to the wing acceleration at the start of a downstroke are more compact and higher in amplitude than those appearing at the end of the downstroke, where a more diffuse pattern of vorticity trails into the upstroke-generated wake. This mid-wing data slice cuts obliquely through a structure shed from the partially retracted wing on the upstroke. Although the structures attributable to the downstroke are much stronger, as confirmed by the stronger induced airflow between them, the upstroke is not completely inactive.

Vertical slices aligned with the mean flow show the spanwise component of vorticity $\omega_y(x,z)$ only, and reconstructing the three-dimensional wake geometry from large numbers of such slices at different spanwise locations is quite lengthy (Spedding et al., 2003b). In particular, streamwise cuts do not show the streamwise vorticity $\omega_x(y,z)$ that trails from the wingtips, except by implication from the changing circulation of coherent patches of $\omega_y(x,z)$. In this paper we focus specifically on cross-comparisons of the $\omega_y(x,z)$ component. For a simple conceptual three-dimensional model, it is a reasonable approximation to imagine that the spanwise vorticity shed at the beginning of the downstroke is continuous with, and approximately the same strength as, the trailing vortices left behind the wingtips during the first half of the downstroke.

The wake geometry in Fig. 3 appears at first sight to be complex, much more so than the simple and elegant models composed of small numbers of vortex lines that one usually sees in flight models (cf. Rayner, 1979; Phlips et al., 1981; Hall and Hall, 1996), and even those of Spedding et al. (Spedding et al., 2003b), where the models are based on such measurements, but in greatly simplified form. There are two reasons for this: first, the wake is imaged quite far away from its origin, and so initial order can be lost in the self-induced deformation of the wake, which includes pairing and merging interactions between same-signed vortices. Second, these wakes at moderate *Re* do not appear like wake models that ignore viscosity. The wake structures interact, deform and dissipate because they live in a real fluid, with viscous forces generated by relative shearing motions. This is as true for fixed wing aerofoils as it is for bird wings.

In Fig. 4, the flow behind a cambered plate and an Eppler 387 wing are compared in vertical planes across the midspan. The spanwise vorticity is shown at a distance $x=1c$ from the leading edge (i.e. immediately behind the trailing edge) and at $x=10c$. At $\alpha=4°$ (the reasons for this choice will become clear later), the near wakes of both aerofoils are very compact chains of alternate-signed vortex patches. For small α, the vortex structures have a passage frequency past an observer fixed in the wind tunnel reference frame of approximately 400 Hz (for the cambered plate), which is

consistent with the laminar free wake instability mechanism modelled and measured by Sato and Kuriki (Sato and Kuriki, 1961). At higher α, the near wake regularity is disrupted by unsteady motion of the trailing edge separation point and from boundary layer instabilities on the pressure side of the aerofoil. In the far wakes (bottom row of Fig. 4), the initial order of the low-α near wake has evolved to a more complex pattern of diffuse vorticity (note the fourfold difference in colourbar scaling). The complexity of fixed wing wakes at moderate downstream distance is not notably less than observed for the flapping bird wake. This is true even when the angle of attack is small so that the early wake at x=1c is very compact and structured. The wing wakes do not look very much like textbook, inviscid descriptions either, and so one would expect the bird wakes to be similarly varied. It might be reasonable to ask why it is that bird wakes do not look more disorganised so far downstream, and this point will be taken up later.

Comparative experiments on the various passerine species flown in the Lund wind tunnel (Hedenström et al., 2006a; Hedenström et al., 2006b; Rosén et al., 2007) have shown that the apparent complexity of the bird wakes does contain structures with readily predictable properties. Surprisingly, some of these properties can be predicted by very simple fixed wing aerodynamic theory. A classical result (see Anderson, 1984) states that the lift per unit span, L', on an aerofoil can be written as:

$$L' = \rho\Gamma U \,, \tag{3}$$

where ρ is the air density, U is the flight speed, and Γ is the strength of the circulation on the wing. Γ is not determined from Eqn 3, but in practice takes a value that is required to avoid physically implausible conditions at the trailing edge. In steady level flight, the total lift, L, must balance the total weight W, and so an expression for Γ can be derived:

$$\Gamma = W / 2b\rho U \,. \tag{4}$$

Eqn 4 gives a prediction for the circulation on a wing of span 2b, flying at steady speed U and supporting a weight, W. As a first approximation, on a wing of finite span, then one will also expect wake vortices of constant strength Γ to be shed from the wingtips as the wing travels forward. Eqn 4 thus can also be used to predict the strength of the most evident wake structures behind a lifting surface, and can be used as the simplest available such model for bird wakes, even though they are not fixed rigid wings.

In comparing flying devices of different sizes and at different flight speeds, it is convenient to non-dimensionalise Γ and dividing Eqn 4 by Uc, we have:

$$\Gamma / Uc = W / \rho U^2 S \,, \tag{5}$$

where S=2bc is the wing planform area. Fig. 5 plots Eqn 5 as a solid line together with data collected from wake experiments on four bird species. They are plotted as a function of U/U_{mp}, where U_{mp} is the estimated minimum power speed for each species, as calculated from a simple actuator disk flight model (Pennycuick, 1989). Its particular value is not important, only that it represents some approximately equivalent speed for each bird. The collapse of data and agreement with the solid line is good. Despite the apparent complexity of the wakes such as shown in Fig. 3, their most simple quantitative measurement is in good agreement with fixed wing theory, as if the wings operate quite like a standard wing, which happens to flap.

Hedenström et al. (Hedenström et al., 2006b) and Rosén et al. (Rosén et al., 2007) also noted that Eqn 5 is very like a lift

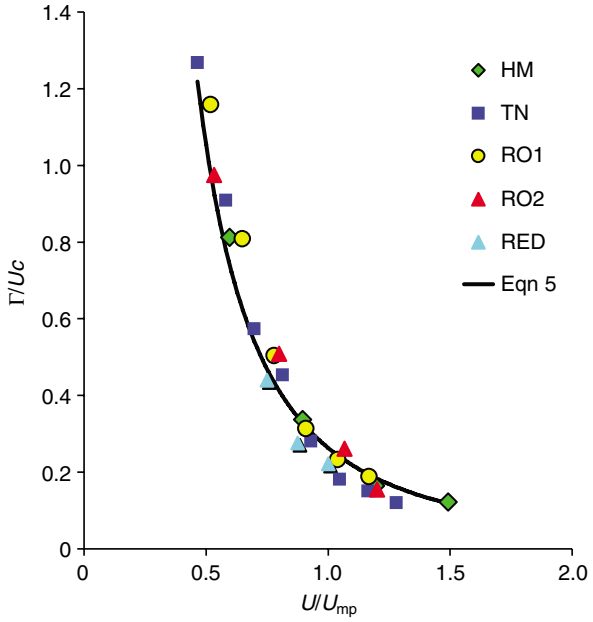

Fig. 5. Normalised circulation, Γ, of the largest coherent wake structure in the wake of a thrush nightingale (TN, squares), two robins (RO, circles and triangles) a house martin (HM, diamonds), and a redstart (RED, shaded triangles) as a function of normalised flight speed (U/U_{mp}). The solid line is from Eqn 5. Data compiled from Rosén et al. (Rosén et al., 2007) and Hedenström et al. (Hedenström et al., 2006b).

coefficient, as can be seen by substituting the dynamic pressure, q=½ρU^2 into Eqn 5, so since W=L,

$$\Gamma / Uc = L / 2qS = C_L / 2 \,. \tag{6}$$

When U/U_{mp}=1, close to some kind of cruising operation, Γ/Uc=0.2, and so all birds in Fig. 5 appear to operate with a time-averaged lift coefficient of approximately 0.4 at U=U_{mp}.

This entire analysis presumes a steady fixed wing, and it is not obvious why the data in Fig. 5 agree so closely with predictions, particularly when the measured wake geometry [see stick figures in Spedding et al. (Spedding et al., 2003b)] clearly differs (as it must) from that of a powered fixed-wing glider. It is possible that the basic wake shape and its strength can be imagined as that of a powered glider, and then that modifications to that basic shape occur due to flapping, so that, on average, steady fixed wing predictions still work. Although no insight can be claimed into the magnitude and importance of the unsteady forces, it does encourage a re-examination of local wing kinematics in a quasi-steady framework.

Wing kinematics in flapping flight

The wingtip trace of the house martin *Delichon urbica* can be well represented by a reconstruction from only two Fourier modes, whose relative amplitude and phase varies with flight speed (Rosén et al., 2007), as shown in Fig. 6. This includes a pause phase, visible as a secondary dip in the vertical component of the wingtip speed, w_{tip}, at the two higher flight speeds of U=8 and 10 m s^{-1}. Fig. 6 shows that the normalised tip speed varies considerably during the course of the wing beat, particularly at the slower flight speeds. The gradients of w_{tip} show the wingtip acceleration, and the peak amplitudes are larger than, or comparable to the flight speed, U. It is clear that an analysis of the local wing section properties must

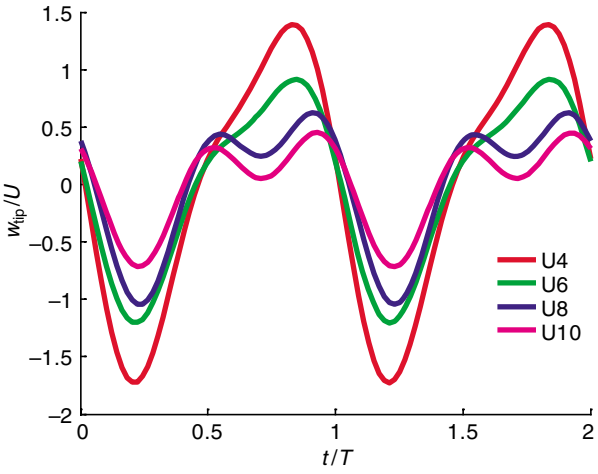

Fig. 6. Normalised vertical wingtip speed plotted over two wing-beat periods (t/T), as reconstructed from the two largest Fourier modes of a series interpolation to kinematic data of the house martin at four flight speeds ($U4$, $U6$, $U8$, $U10$) from Rosén et al. (Rosén et al., 2007).

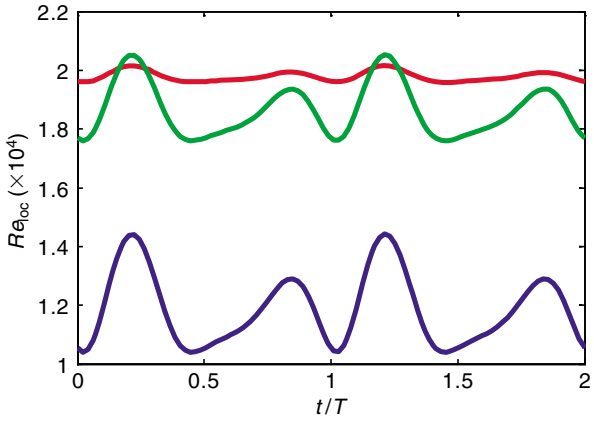

Fig. 7. Local wing section Reynolds number (Re_{loc}) over two wing-beat cycles (t/T) for U=6 m s^{-1} at three spanwise locations; r=0.2b (red, upper curve), 0.5b (green, middle curve) and 0.8b (blue, lower curve), where b=wing semispan).

therefore take into account this variation, and a local Reynolds number, Re_{loc}, can be calculated from:

$$Re_{loc}(r) = \frac{|\vec{u}_{loc}(r)|c(r)}{\nu} \quad (7)$$

where $c(r)$ is the wing chord length at position r along the semispan, b, $u_{loc}(r)$ is the local relative air speed (which depends on w_{tip} and U) incident on the wing section at position r, and ν is the kinematic viscosity. $u_{loc}(r)$ is not measured, but estimated, from a wing model that assumes a rigid wing flapping at a single hinge at the root and with kinematics given by the Fourier coefficients responsible for Fig. 6. This simple wing model allows a quick estimate of the approximate conditions on the wing at different spans, shown in Fig. 7 for r=0.2b, 0.5b and 0.8b.

Re_{loc} fluctuates much as w_{tip} fluctuates, but the amplitude of the fluctuations is much smaller at the wing root, where, because of the higher mean chord, Re_{loc} is actually highest. Here, Re_{loc} is still less than 2×10^4, however, and it falls to even lower values towards the tip, and Re_{loc} at r=0.8b is usually less than 1.4×10^4. This example is for U=6 m s^{-1}, which is slightly below an estimated cruising speed, U_{mp}=8.5 m s^{-1}. However, it shows that for the small-sized passerines whose aerodynamic performance has been measured thus far, local Reynolds numbers are on the lower end of the range considered in Fig. 1. The difference is important because the propensity for laminar boundary layer separation and the possibility for its reattachment on the wing is very strongly affected by Re.

Aerodynamic performance of wing sections at moderate Re

Here we summarise properties of time-averaged lift:drag polars for fixed wings, measured for values of Re and AR that are similar to those for small bird wings. The implied positions of time-averaged performance of the birds will be noted on these steady-state polars. Although bird wing aerodynamics are not always likely to be well described on a time-averaged basis (particularly at low flight speeds), comparing their average performance on average polars is at least a consistent operation, and the results might be instructive. It should also be noted carefully that even though time-averaged performance calculations might appear to be consistent, it still does not mean that they are actually correct, and still further does not mean that instantaneous forces and/or unsteady effects are not important. The purpose is restricted solely to examining the degree of agreement that can be explained using the most simple and parsimonious model.

Fig. 2 showed that as Re drops from 10^5 to 6×10^4, the performance characteristics of an aerofoil such as the Eppler 387 change dramatically. Fig. 8, from measurements in the USC Dryden wind tunnel, show that the performance characteristics change again as Re continues to drop. Recall that Fig. 7 suggests that Re_{loc}, the local Reynolds number on any wing section, falls mostly between 1 and 2×10^4. Fig. 8 shows that at such low Re, the curve of $C_L(C_D)$ for a wing with AR=6 is quite smooth, in strong contrast to the abrupt jumps (in both C_D and C_L) seen at higher Re. As Re falls, $C_{L,max}$ also falls considerably, but this is most likely irrelevant to the cruising bird. Recall further that the wake measurements of Fig. 5 suggest a performance that is commensurate with a time-averaged lift coefficient of approximately 0.4. The horizontal line drawn at C_L=0.4 in Fig. 8 shows how this positions the wing comfortably below regions where C_D rises steeply. Fig. 9 shows that the angles of attack required for an AR=6, Eppler 387 wing to generate these moderate lift coefficients are 4, 3, 2.5 and 1° for Re=1, 2, 3 and 6×10^4, respectively. The higher the Reynolds number, the smaller the required angle of attack for a given lifting performance, and the more conservative a regime that can be occupied.

Discussion

Inferring wing section properties of bird wings

This paper is centred around the medium-speed, or cruising performance, of bird wings. The first example result in Fig. 3 showed that the far wake is moderately complex in appearance. However, given the complexity of similar far wakes of simple wing shapes in Fig. 4, the bird wake begins to look comparatively simple, and the strengths of the largest coherent vortex patches are quite simple to predict, based only on classical wing theory arguments (Fig. 5). The normalised wake circulation, Γ/Uc, is very well matched by predictions for fixed wings of the same size, carrying the same load, and flying at the same speed. Indeed, Γ/Uc can be

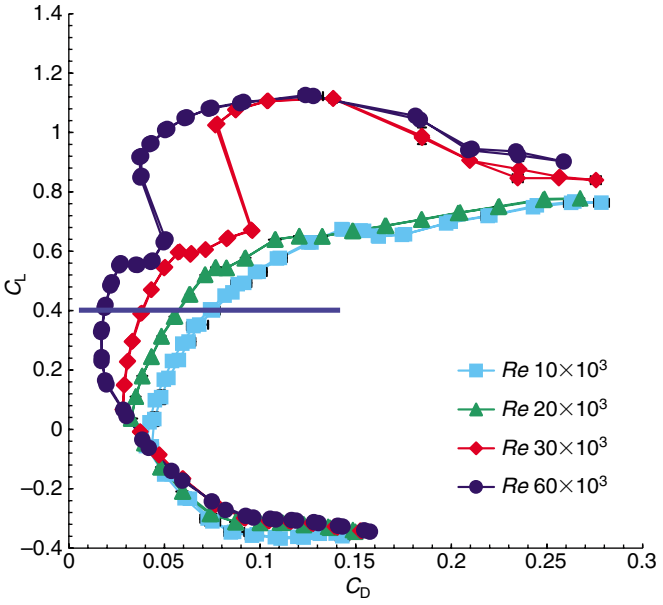

Fig. 8. Lift:drag polars for the Eppler 387 wing at Reynolds numbers ranging from approximately 1×10^4 to 6×10^4. Each $C_L(C_D)$ curve is plotted twice, for increasing and decreasing α from –12°–19°. The two sets of curves cannot be distinguished. Blue horizontal line marks the preferred C_L of the wing.

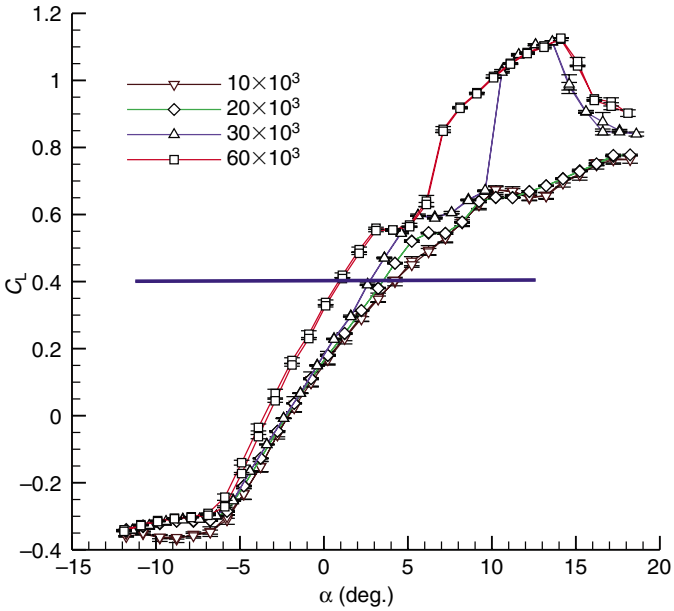

Fig. 9. C_L as a function of angle of attack, α, for the Eppler 387 wing. Blue horizontal line, see Fig. 8.

expressed as one half of the time-averaged lift coefficient (Eqn 6), and its quite moderate value, approximately 0.4 at U_{mp}, suggests, in turn, a wing that is at commensurately moderate angles of attack. The fixed wing wake results of the cambered plate and Eppler 387 aerofoil in Fig. 4 are therefore quite likely to be representative of the types of flow that can be expected in the bird wake.

In the Introduction, it was noted that wing performance at moderate *Re* is notoriously sensitive to both *Re* and to small changes in geometry and environmental conditions. However, in deducing likely local sectional Reynolds numbers Re_{loc} in Fig. 7, it appears that for these small birds, Re_{loc} is just below values where the aerodynamic performance becomes strongly affected by the stability and transitional flows in and around laminar separation bubbles (Fig. 8). The lowest Re_{loc}, where fixed wing properties are the most stable, are found at the wingtips, and the higher Re_{loc} are found towards the root, where the oscillation amplitude is at its lowest.

The detailed wake measurements discussed here are available only for small-sized birds, occupying the lower *Re* regime of all birds in Fig. 1, and it is reasonable to wonder how these results scale as the size and mean-chord Reynolds number increase. If the fixed wing flight model remains correct, at least to a first order of approximation, then Eqn 6 implies that the dimensionless lift coefficient, C_L, will also be constant for a given U/U_{mp}. The angle of attack required to achieve $C_L\approx0.4$ decreases as *Re* increases (Fig. 9), and so as *Re* increases from values of 1×10^4 where the steady-state flow is always stable, to 6×10^4 where abrupt performance jumps appear due to flow separation and subsequent reattachment, so the required angle of attack falls to move the cruising performance point further away from the unstable region. It is also notable that when *Re* does rise sufficiently to bring the wing into a regime that has performance jumps due to separation, the cruising angle of attack is never more than a couple of degrees beneath the point at which these effects come into play. Thus, small changes in angle of attack can produce large changes in the force direction and magnitude on the wing. This would be a useful condition for control purposes.

It should be noted clearly that the arguments here are that one can understand something of the aerodynamics of the complex, deformable, feathered, flapping wings by comparing predictions from simple fixed, rigid wing models. Even when flapping motions are considered, they are for a rigid wing of the same size, flapping about a simple hinge at the root. The idea is not that such simplifications can provide a complete or even sufficient explanation of the true wing geometry and motions, but that since the quantitative data and observations do agree well with model predictions based on fixed wings, this approach shows the simplest tenable baseline approximation, upon which more complex and realistic theories might be constructed.

What fixes the Strouhal number?

The inverse of the ratio of wingtip speed to forward flight speed is commonly termed an advance ratio, which indicates the forward distance travelled relative to the tip motion of an oscillating or rotating propulsor. While Fig. 6 shows that w_{tip}/U varies greatly during the course of a wing beat, the time-averaged (root mean square) value can be a convenient measure of the relative importance of flows induced by the unsteady wing motion compared with the steady (approximately constant) flight speed. It is very simply related to another common measure of relative timescales in unsteady wakes, the Strouhal number *St*:

$$St = fA / U\,, \tag{8}$$

where A is either the maximum lateral distance between shed vortices in an unsteady wake, or the tip-to-tip amplitude of an oscillating (flapping, or heaving/pitching) wing. The average $\overline{w}_{tip}/U$ can be expressed as:

$$\frac{\overline{w}_{\mathrm{tip}}}{U} = \frac{A}{T/2} \times \frac{1}{U} = \frac{2A}{UT} \ , \qquad (9)$$

for a wingtip that travels a vertical distance of A twice every wingbeat period, T. The right hand side of Eqn 9 re-expresses the ratio of speeds on the left hand side as a ratio of distances, where $2A$ is the wingtip travel distance and UT is the horizontal distance covered at speed U during one wing beat. From Eqn 8 and 9,

$$\overline{w}_{\mathrm{tip}}/U = 2St \ . \qquad (10)$$

It has been noted previously (Rosén et al., 2004) that since both f and A tend to vary little with U, then St (or any equivalent measure) just decreases as $1/U$, and is not constant for any given bird over its range of natural flight speeds.

The Strouhal number tends to fall within a restricted range of possible values for flying birds, bats and insects alike, taking values between 0.2–0.4, with a mean of 0.29 in a literature sample for animals flying at reported preferred flight speed (Taylor et al., 2003); the median value for 'direct' fliers (birds that do not practice intermittent flight) was 0.2. Interestingly, the root mean square of the varying $w_{\mathrm{tip}}/U(t)$ in Fig. 6 shows that $\overline{w}_{\mathrm{tip}}/U$ is 0.71 for U=6 m s^{-1} and 0.54 for U=8 m s^{-1} for the house martin. This is equivalent to St=0.35 and 0.27, respectively, and since a 'preferred' flight speed most likely lies between these two values (Rosén et al., 2007), then the equivalent St=0.31, has a value not inconsistent with Taylor et al.'s analysis.

Explanations for the observed $0.2 \leqslant St \leqslant 0.4$ range in animal swimming and flying propulsion have concentrated on unsteady mechanisms (see also Wang, 2000), which can most generally be described as requiring a balance between time scales of growth and then separation of leading edge vortices and time scales of the oscillating propulsor motion itself. Wang also describes the constraint on St (finding preferred values between 0.16 and 0.27) in terms of the maximum angle of attack without stall, but these maximum angles are from 45°–60° and are for an unsteady stall in a viscous flow at Re=10^3 dominated by large-scale separation.

From wing kinematic constraints alone (i.e. ignoring the contributions due to induced flow by the wing itself) the local aerodynamic angle of attack is determined by a combination of the stroke plane angle, the local twist and the section speed relative to the mean flow (Fig. 10). For the purposes of argument, let us suppose that the local aerodynamic angle of attack is fixed during each wingstroke. We may then describe the stroke plane angle and local twist together as a summed quantity, α_0, which is constrained mechanically to operate within a certain range. Then the aerodynamic angle of attack, α, is:

$$\alpha = \alpha_0 + \alpha_{\mathrm{w}} \ , \qquad (11)$$

where α_{w} is simply related to $\overline{w}_{\mathrm{tip}}/U$ by:

$$\alpha_{\mathrm{w}} = \arctan(\overline{w}_{\mathrm{tip}}/U) \ , \qquad (12)$$

as can be seen from Fig. 10. So, operating a flapping wing at a preferred α depends on the tip speed to forward speed ratio, which is proportional to St. The tendency to maintain a constant St close to U_{mp} (or other measure of preferred flight speed) can be seen as simply the maintenance of a low positive angle of attack at which the wing section performance is efficient (in terms of L/D) and safe (in avoiding abrupt separation). The fact that St is not actually constant over the range of U for any given bird shows that α_0 is not constant either, but is tailored to adapt to the varying advance ratio. For the foregoing argument to apply, we need not require that α_0 be constant, only that it has a fixed range, which is similar amongst the different species, and that the preferred flight speed condition occurs at the centre of that range.

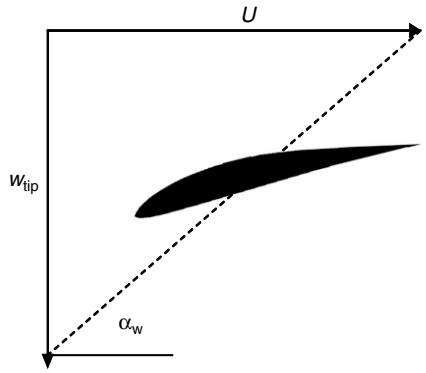

Fig. 10. The local wing section angle of attack depends on the ratio of w_{tip} to U, and on a local rotation, which depends on the stroke plane angle and local twist. Silhouette shows a generic wing cross section at same span location.

The maintenance of a small local angle of attack along a flapping wing is analogous to control of the proportional feathering parameter identified by Lighthill (Lighthill, 1969; Lighthill, 1970) for efficient propulsion in oscillating fins, and extended to three-dimensional geometries (Karpouzian et al., 1990). In birds, St is allowed to vary with U, so that both f and A can be maintained almost constant. The variation is possible because variation in α_0 can give reasonable values of α, despite the variation in α_{w}. The tendency to constant St at some preferred flight speed is a result of operating in the middle of the range of available α_0. The comparatively simple form of the measured bird wakes, even when measured far downstream (Fig. 3) indeed strongly suggests a fine degree of boundary layer control through manipulation of local α, so that large-scale separation at the trailing edge, and its attendant shedding into the wake, are avoided.

Limitations

The preceding analysis applies observations from fixed wings, with simple shape, to the unsteady problem of flapping bird wings, with complex and time-varying shape. The justification for so doing is provided partly by the reasonable agreement between simple steady aerodynamic models and the gross overall features in the bird wake. The paper thus advances the simplest explanation for the observations. This is not to assert that unsteady aerodynamics must play no role, nor that significant dynamic separation effects cannot occur. Even when taking into account the wing kinematics themselves, we have applied a quasi-steady approach, where at each instant wing sections are analysed as if they had the same properties had they been frozen in time at each instant. The insufficiency of this quasi-steady approach in low speed and/or hovering flight has been famously demonstrated (Norberg, 1976; Ellington, 1984a; Ellington, 1984b), and a more detailed quantitative analysis from flapping and translating models in a tow tank has been published (Sane and Dickinson, 2002; Dickson and Dickinson, 2004). There will likely be interesting unsteady phenomena, possibly involving momentary flow separation, that contribute significantly to a fuller understanding of the aerodynamics of bird wings, but the current results, for the particular case of cruising flight at mean chord Reynolds numbers between 5 and 10×10^4, suggest that fixed wing behaviour can explain much.

Not all airfoil sections behave as the Eppler 387 does, which makes an interesting test case in the severity of the separation bubble effects, but is not necessarily representative of wing sections that are actually designed for $Re<10^5$. Although this type of behaviour is common for smooth aerofoils with finite thickness, many low-*Re* aerofoils, such as the Davis 3R (Lyon et al., 1997), are significantly thinner and have fewer problems in large drag performance variations. Their section profiles are more similar to the cambered plate of Fig. 4, which has superior *L*/*D* to the Eppler 387 when $Re<10^5$ (Spedding et al., 2006), and further research will be carried out on such shapes, where now the instantaneous flow field can be measured as well as time-averaged forces. A more detailed consideration of the combination of variation in section shape and local angle of attack with time and along the span in real flapping wings will be required to fully demonstrate the aerodynamic flow control that is suggested in rather crude terms here.

Conclusions

The flow around and behind simple fixed wings at Reynolds numbers similar to bird flight is not necessarily simple itself, and the wakes of flying birds are not significantly more complex than that. This observation suggests that simple aerodynamic models might help to understand many features of bird flight, as complex kinematics and geometry are reduced to simple principles. One of these simple principles might be that the constant Strouhal number arguments advanced for flapping wing flight can be explained as a simple consequence of maintaining a moderate angle of attack on the lifting wing (or propelling tail). The data presented are for small birds, because they are easiest to study in facilities with finite size. Since the performance characteristics of fixed wings vary significantly with Reynolds number, the design constraints suggested here may apply only to a fixed range of sizes, and we may find that larger bird wings are designed differently.

List of symbols and abbreviations

The dimensions are given in terms of mass, M, length, L and time, T.

$\{u,v,w\}$	L/T	disturbance velocities in $\{x,y,z\}$
$\{x,y,z\}$	L	streamwise, spanwise and vertical directions
A	L	tip-to-tip wingbeat amplitude
AR		wing aspect ratio ($=2b/c$)
b	L	wing semispan
c	L	mean chord length in flightwise direction
C_d		section drag coefficient
C_D		wing drag coefficient
C_L		wing lift coefficient
C_p		section lift coefficient
f	1/T	wingbeat frequency
g	L/T^2	acceleration due to gravity
l	L	characteristic length
L	$M.L.T^{-2}$	lift
m	M	body/aircraft mass
q	M/LT^2	dynamic pressure
r	L	position along wingspan
Re		Reynolds number ($=Uc/\nu$)
Re_{loc}		local Re
S	L^2	wing planform area
St		Strouhal number ($=fA/U$)
t	T	time
T	T	wingbeat period
U	L/T	flight speed
u_{loc}	L/T	local incident velocity on a wing section
U_{mp}	L/T	estimated flight speed for minimum power
u'	L/T	root mean square of velocity fluctuations
W	$M.L.T^{-2}$	bird/aircraft weight ($=mg$)
w_{tip}	L/T	vertical component of wingtip speed
α	deg.	aerodynamic angle of attack
α_0	deg.	local twist from stroke plane
α_w	deg.	local α due to vector sum of U and w_{tip}
δt	T	small time interval (DPIV effective exposure time)
Γ	L^2/T	circulation/strength of a vortex patch, or on a lifting wing
λ		wavelength
μ	M/LT	viscosity
ν	L^2/T	kinematic viscosity ($=\mu/\rho$)
ρ	M/L^3	air density
ω_i	1/T	vorticity component in the ith direction $\{i=x,y,z\}$

References

Althaus, D. (1980). *Profilpolaren für den Modellflug.* Karlsruhe: NeckarVerlag.

Anderson, J. D. (1984). *Fundamentals of Aerodynamics.* New York: McGraw-Hill.

Dickson, W. B. and Dickinson, M. H. (2004). The effect of advance ratio on the aerodynamics of revolving wings. *J. Exp. Biol.* **207**, 4269-4281.

Ellington, C. P. (1984a). The aerodynamics of hovering insect flight. I. The quasi-steady analysis. *Philos. Trans. R. Soc. Lond. B Biol. Sci.* **305**, 1-15.

Ellington, C. P. (1984b). The aerodynamics of hovering insect flight. IV. Aerodynamic mechanisms. *Philos. Trans. R. Soc. Lond. B Biol. Sci.* **305**, 79-113.

Fincham, A. M. and Delerce, G. (2000). Advanced optimization of correlation imaging velocimetry algorithms. *Exp. Fluids* **29**, 13-22.

Fincham, A. M. and Spedding, G. R. (1997). Low-cost, high resolution DPIV for measurement of turbulent fluid flow. *Exp. Fluids* **23**, 449-462.

Hall, K. C. and Hall, S. R. (1996). Minimum induced power requirements for flapping flight. *J. Fluid Mech.* **323**, 285-315.

Hedenström, A., Rosén, M. and Spedding, G. R. (2006a). Vortex wakes generated by robins *Erithacus rubecula* during free flight in a wind tunnel. *J. R. Soc. Lond. Interface* **3**, 263-276.

Hedenström, A., Griethuijsen, L., Rosén, M. and Spedding, G. R. (2006b). Vortex wakes of birds: recent results using particle imaging velocimetry. *Anim. Biol.* **56**, 535-549.

Hoerner, S. F. (1965). *Fluid-Dynamic Drag.* New Jersey: Hoerner Fluid Dynamics.

Karpouzian, G., Spedding, G. R. and Cheng, H. K. (1990). Lunate-tail swimming propulsion. Part 2. Performance analysis. *J. Fluid Mech.* **210**, 329-351.

Laitone, E. V. (1997). Wind tunnel tests of wings at Reynolds numbers below 70 000. *Exp. Fluids* **23**, 405-409.

Lighthill, M. J. (1969). Hydromechanics of aquatic animal propulsion. *Annu. Rev. Fluid Mech.* **1**, 413-446.

Lighthill, M. J. (1970). Aquatic animal propulsion of high hydromechanical efficiency. *J. Fluid Mech.* **44**, 265-301.

Lyon, C. A., Broeren, A. P., Giguere, P., Gopalarathnam, A. and Selig, M. S. (1997). *Summary of Low-Speed Airfoil Data, Vol. 3.* Virginai Beach, VA: Soartech.

Norberg, U. M. (1976). Kinematics, aerodynamics and energetics of horizontal flapping flight in the long-eared bat (*Plecotus auritus*). *J. Exp. Biol.* **65**, 179-212.

Pennycuick, C. J. (1989). *Bird Flight Performance: A Practical Calculation Manual.* Oxford: Oxford University Press.

Pennycuick, C. J., Alterstam, T. and Hedenström, A. (1997). A new low-turbulence wind tunnel for bird flight experiments at Lund University, Sweden. *J. Exp. Biol.* **200**, 1441-1449.

Phlips, P. J., East, R. A. and Pratt, N. H. (1981). An unsteady lifting line theory of flapping wings with application to the forward flight of birds. *J. Fluid Mech.* **112**, 97-125.

Rayner, J. M. V. (1979). A vortex theory of animal flight. II. The forward flight of birds. *J. Fluid Mech.* **91**, 731-763.

Rosén, M., Spedding, G. R. and Hedenström, A. (2004). The relationship between wingbeat kinematics and vortex wake of a thrush nightingale. *J. Exp. Biol.* **207**, 4255-4268.

Rosén, M, Spedding, G. R. and Hedenström, A. (2007). Wake structure and wingbeat kinematics of a house-martin *Delichon urbica*. *J. R. Soc. Interface* **4**, 659-668.

Sane, S. P. and Dickinson, M. H. (2002). The aerodynamic effects of wing rotation and a revised quasi-steady model of flapping flight. *J. Exp. Biol.* **205**, 1087-1096.

Sato, H. and Kuriki, K. (1961). The mechanism of transition in the wake of a thin flat plate placed parallel to a uniform flow. *J. Fluid Mech.* **3**, 321-352.

Schmitz, F. W. (1945). *Aerodynamik des Flugmodells.* Duisberg: Karl Lange.

Spedding, G. R., Hedenström, A. and Rosén, M. (2003a). Quantitative studies of the wakes of freely-flying birds in a low-turbulence wind tunnel. *Exp. Fluids* **34**, 291-303.

Spedding, G. R., Rosén, M. and Hedenström, A. (2003b). A family of vortex wakes generated by a thrush nightingale in free flight in a wind tunnel over its entire natural range of flight speeds. *J. Exp. Biol.* **206**, 2313-2344.

Spedding, G. R., McArthur, J., Rosén, M. and Hedenström, A. (2006). Deducing aerodynamic mechanisms from near- and far-wake measurements of fixed and flapping wings at moderate Reynolds number. *AIAA* Paper 7783.

Taylor, G. K., Nudds, R. L. and Thomas, A. L. R. (2003). Flying and swimming animals cruise at a Strouhal number tuned for high power efficiency. *Nature* **425**, 707-711.

Wang, J. Z. (2000). Vortex shedding and frequency selection in flapping flight. *J. Fluid Mech.* **410**, 323-341.